Femtosecond Dynamics of Double Proton Transfer in a Model DNA Base Pair: 7-Azaindole Dimers in the Condensed Phase

T. Fiebig, M. Chachisvilis, M. Manger, and A. H. Zewail*

Arthur Amos Noyes Laboratory of Chemical Physics, Laboratory for Molecular Sciences, California Institute of Technology, Pasadena, California 91125

A. Douhal, I. Garcia-Ochoa, and A. de La Hoz Ayuso

Departamento de Química Física, Facultad de Químicas, Sección de Toledo, Universitad de Castilla-La Mancha, San Lucas, 3, 45002, Toledo, Spain

Received: June 3, 1999

The dynamics of double proton transfer in 7-azaindole (7-AI) dimers, a model DNA base pair, are investigated in real time using femtosecond transient absorption and fluorescence upconversion techniques. In nonpolar solvents we examine the isotope effect, the excitation energy dependence, and the structure analogue of the tautomer (7-MeAI). A detailed molecular picture of the nuclear dynamics in the condensed phase emerges with the relationship to the dynamics observed in molecular beams: Following the femtosecond excitation there are three distinct time scales for structural relaxation in the initial pair, proton (hydrogen) transfers, and vibrational relaxation or cooling of the tautomer. The molecular basis of tunneling and concertedness are elucidated by careful examination of the isotope effect and the time resolution. Comparison with the results in the isolated pair indicates the critical role of the N−H and N···N nuclear motions in determining the effective potential, and the thermal excitation in solution. Because the barrier is small, ∼1.3 kcal/mol, both are important factors and experiments at much higher energies will be unable to test either tunneling or concertedness. Finally, we compare the experimental results and the dynamical picture with detailed ab initio and molecular dynamics simulations.

I. Introduction

Because of its unique energy and directional force, the hydrogen bond plays a central role in a wide variety of chemical and biological phenomena with characteristics beyond those of the covalent bond. One such characteristic is the tautomerization involving two or more hydrogen bonds. Since the discovery in 1953 of the structure of the DNA double helix by Watson and Crick,[1] this aspect of tautomerization as a cause of mutation in DNA hydrogen-bonded base pairs have been the subject of numerous studies.[2] This cause of errors (mutagenesis) in DNA replication is similarly considered for photoinduced proton-transfer reactions. The theoretical description is based on prototype models of quantum tunneling.[3] Experimental studies of model systems are desirable for the aim of understanding the fundamental elementary steps of multiple proton transfer in complex molecular networks.

7-Azaindole (7-AI), a bicyclic aza-aromatic molecule, has a number of interesting properties. It is isoelectronic with purine and has a close relationship with the nucleic bases adenine and guanine. Furthermore, 7-AI forms dimers (Scheme 1) which show structural similarities with the adenine-thymine (A-T) and guanine-cytosine (G-C) base pairs in DNA; all three complexes are joined by two (or three) hydrogen bonds. Consequently, 7-AI is a unique model system for photoinduced double proton-transfer processes in biological systems. Moreover, this dynamics of multiple, hydrogen-bonded systems is also important to the understanding of time scales in molecular recognition and supramolecular chemistry.[4]

SCHEME 1

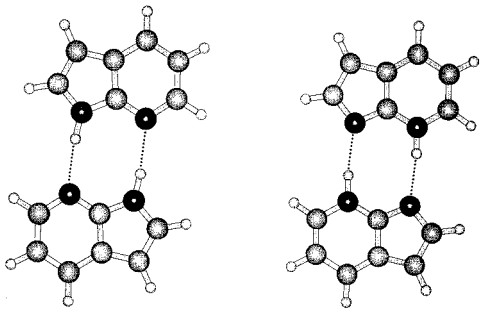

Excited-state proton transfer in 7-AI dimers was first reported by Taylor, El-Bayoumi, and Kasha.[5] In subsequent investigations, Ingham et al.[6,7] studied the effects of temperature and deuterium substitution which enabled them to estimate the barrier height for proton transfer (1.4 kcal/mol) and suggest that quantum mechanical tunneling is involved, at least at low temperatures. Since then, much work[8−11] has been done and in different solvents. The work by Itoh and co-workers in solution provided information about some important properties of the tautomer ground state of both 7-AI dimer and monomer species; the ground-state tautomer lifetimes of 17 and 47 μs were obtained for dimer and monomer, respectively.[11] Studies were also made in matrices at 4.2 K by Ingham et al.[7] and in supersonic-jet expansions by Fuke et al. and Nakayuma et

10.1021/jp991822p CCC: $18.00
Published on Web 08/31/1999

al.[12−14] The work by Fuke et al.[13] suggested two dimer structures, one reactive (i.e., undergoing proton-transfer reactions) and another nonreactive. An important conclusion was that the proton transfer is coupled to the N−H···N stretching vibration in the hydrogen bond.

Time-resolved studies on the picosecond time scale began with the work of Hetherington et al.[15] who found that the transfer takes place on a time scale shorter than 5 ps. They suggested two tautomerization pathways, a direct one from nonequilibrated dimers and an indirect pathway from thermally equilibrated dimers. With the aid of improved subpicosecond time resolution (∼0.3 ps), Share et al.[16] were able to obtain the time constant of 1.4 ps for the protonated and 4.0 ps for the deuterated species. It was suggested that another channel, forming the ground-state tautomer, is operative on the time scale of the laser pulse width.

With femtosecond (fs) resolution, we reported our first study of the tautomerization dynamics of 7-AI dimers in a molecular beam using femtosecond-resolved mass spectrometry.[17] The results, which were obtained for different available energies and isotopic composition, showed the time scales for the transfer in the isolated pair and a striking isotope effect, even when the vibrational energy was near zero in the dimer; the vibrational and rotational temperatures in the molecular beam are very low, typically 10−20 and 2−5 K, respectively. Accordingly, we suggested tunneling with the process occurring in a two-step mechanism: the first proton transfer takes places on a time scale of a several hundred femtoseconds, whereas the second proton transfer is slower, occurring on the picosecond time scale. It was pointed out that the issue of concertedness must be addressed by considering (at least) a two-dimensional energy surface to account for the both symmetric and asymmetric nuclear motions.[17] Folmer et al.,[18] in an elegant set of experiments involving the technique of Coulomb explosion, arrested the intermediate. They found that the intermediate is formed in ∼700 fs and decayed on the picosecond time scale, in agreement with the study made in this laboratory using femtosecond-ionization mass spectrometry.[17] The results of refs 17 and 18 are also consistent with the photoelectron studies by Lopez-Martens et al.[19] as discussed below.

Theoretical studies of isolated 7-AI were also reported by several groups. Douhal et al.[20] carried out ab initio calculations reporting the presence of an intermediate in the excited state of the dimer. Guallar et al.[21] performed ab initio calculations and concluded that an asymmetric geometry corresponding to a highly localized excitation in the S_1 state results in stronger hydrogen bonds and thus is energetically more favorable. Both of these results are consistent with a nonconcerted reaction mechanism. Guallar, Batista, and Miller[22] provided the first dynamical calculation using full quantum and semiclassical methods. As discussed below, they show that in the isolated molecule (dimer) the double proton transfer is *sequential*, involving two steps; the concerted route is relatively much higher in energy. The wave packet motion in the space of the proton displacement and intermonomer symmetric coordinates indicates that the *first* proton transfer (with tunneling) occurs in time steps of about 200 fs; there are nuclear relaxations and reorganization which occur on the 100 fs time scale. Additionally, two significant points were made: First, the finding that the intermediate is mostly covalent in character, i.e., not zwitterionic, and second, that the initial excitation is dominantly a HOMO−LUMO (L_a) transition localized on one of the monomer sites.

In solution, studies of 7-AI were carried out by Takeuchi et al.[23,24] and by us,[25] using the technique of femtosecond fluorescence upconversion. In both studies the authors were able to resolve a 1 ps decay component and a 1 ps rise component which gives the effective rate of the formation of the tautomer. In addition, we have also observed a slower 12 ps rise component in the tautomer fluorescence and a significant isotope effect. In solution, however, one must consider the influence of the solvent on energy redistribution and vibrational relaxation, *and* the major difficulty of the isotopic exchange with residual water of the environment.

SCHEME 2

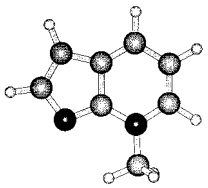

Tautomer Analogue (7-MeAI)

In this paper, we give a full account of our experimental and theoretical studies of double proton transfer dynamics of 7-AI dimers in solution, with a comparison of earlier gas-phase studies. Armed with studies of both transient absorption and fluorescence upconversion on the femtosecond time scale we investigate the effect of isotopic substitution (using a new method for 7-AI) and the excited-state dynamics of 7-MeAI (Scheme 2), an analogue of the tautomer.

Finally, we report ab initio calculations of the reaction pathways along both proton coordinates in the base pair to elucidate the nature of reactive intermediates and transition states. The paper is structured as follows: In section II, we describe the experimental techniques, sample preparation and the synthesis of deuterated 7-AI and 7-MeAI. The experimental results are presented in section III, followed by the discussion in section IV.

II. Experimental Section

A. Femtosecond Fluorescence Upconversion. The fluorescence upconversion experiments were performed with a setup which is shown schematically in Figure 1A. The system consists of a femtosecond Ti:sapphire oscillator coupled to a regenerative amplifier which generates 90 fs, 0.6 mJ light pulses. The pulses are centered around 798 nm at 1 kHz repetition rate. A beam splitter was used to divide the light beam into the excitation and gating branches with a 4 to 1 ratio. The excitation pulses were tripled to yield 266 nm pulses using two 0.2 mm BBO crystals. These pulses were subsequently compressed, using two silica prisms to compensate for group velocity dispersion, and focused into the sample.

The sample flowed through a jet. This arrangement was introduced to minimize the effects of laser-induced photochemistry. We have found that it is advantageous to use a jet because the photoproducts tend to form a film on the quartz windows of the flow cell; the film is highly emitting in the region of interest. Typically, the energy of the excitation pulse at the sample was ∼30 nJ. At these energies, the fluorescence signal from our samples was linearly dependent on the excitation intensity. To examine the population dynamics, the polarization of the excitation light was set at the magic angle with respect to that of the gating pulse. We also studied carefully the behavior of the signal in (||, ||) and (||, ⊥) configurations to examine the role of the anisotropy. The experiments with excitation wavelength at 310 nm were carried out using an optical parametric amplifier (OPA).

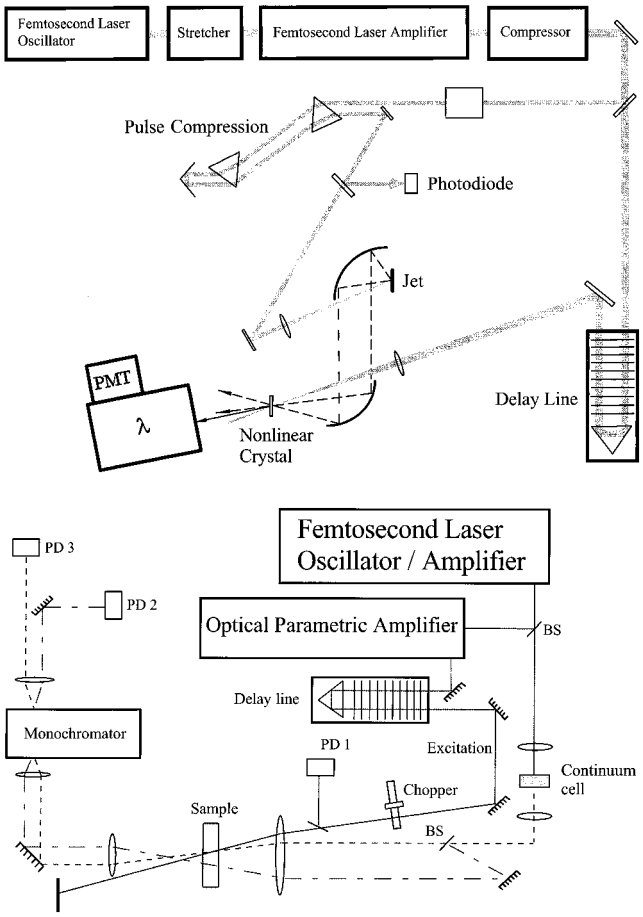

Figure 1. (A, top) The experimental arrangement for the femtosecond fluorescence upconversion measurements. (B, bottom) Experimental arrangement for femtosecond transient absorption measurements.

The sample fluorescence was collected and focused into a nonlinear crystal (0.2 mm, BBO, type I) using reflective optics. The gating pulse was time delayed and also focused into the nonlinear crystal to overlap with the sample fluorescence. The resulting sum-frequency signal in the UV region was filtered using a double monochromator and detected with a photomultiplier tube. When necessary, the signal was also normalized to the energy of the excitation pulse. The temporal response function of the pulses and detection is ~300 fs. Since the pulse width is 90 fs, the resolution is only limited by the detection system. The signal was monitored for different delay times and processed with a computer-aided interface arrangement.

B. Femtosecond Transient Absorption. The transient absorption experiments were performed with a setup which is shown schematically in Figure 1B. The femtosecond system, which generates 90 fs, 0.6 mJ light pulses, is similar to that described above, but the experimental arrangement is entirely different. The pulses from the amplifier were divided into two parts with a 5 to 1 ratio. The weaker beam was employed for generation of white-light continuum to serve as probe light. The continuum was generated by focusing the 50 μJ pulses into a 1 cm water-flow cell. The continuum light was then collimated using quartz optics and divided by a 35/35 broad-band beam splitter into the *probe* and *reference* beams. The stronger beam was used to pump the OPA. The output from the OPA was frequency doubled two times to produce excitation pulses in the UV region (320 nm). The polarization of the excitation light was set at the magic angle with respect to that of the probe light. The response function of the apparatus is limited only by the 90 fs pulse width.

The three beams, *excitation*, *probe*, and *reference*, were focused into the sample with a quartz lens ($f \approx 10$ cm), but only the excitation and signal beams were overlapped in the sample which was flowed in the 1 mm quartz cell. After the sample, both signal and reference beams were focused into a monochromator and detected using silicon photodiodes (PD2, PD3) which are capable of recording separately each laser pulse. The chopper in the excitation beam was used to block excitation of the sample for measuring the background optical density, while photodiode PD1 was used to monitor the energy of the excitation beam.

Typically, it was possible to measure changes of optical density on the order of 10^{-4}, after averaging the signal from ~1000 pulses for each delay position. All experiments were carried out at room temperature. Using the filtered white light continuum, experiments were carried out for different probe wavelengths. The signal was recorded as a function of delay times and processed with a computer-aided interface arrangement.

C. Steady-State Absorption and Fluorescence. Steady-state absorption spectra were measured using Cary 50 (Varian Inc.) spectrophotometer. Typically, a 0.1 mm quartz optical cell was used. The fluorescence spectra of $\sim 10^{-2}$ M solutions of 7-AI were recorded on Fluoromax-2 spectrophotometer in an arrangement where front surface illumination and detection were used. The fluorescence of monomer 7-MeAI was measured in a 1 cm quartz cell using a standard detection configuration.

D. Sample Preparation and Characterization. 7-AI (98% purchased from Aldrich Inc.) was purified by vacuum sublimation. The solvents, 3-methylpentane (from Aldrich Inc.), diethyl ether (from EM Industries Inc.), and chloroform-*d* (from Cambridge Isotope Laboratories Inc.), were dried according to known procedures and distilled before use. As reported earlier,[25] upon laser excitation, 7-AI forms some photoproducts which tend to stick on the surface of the cell. Accordingly, the fluorescence upconversion experiments were carried out in a jet system containing only Teflon and glass parts. For the transient absorption measurements we used a quartz cell (1 mm) which was moved slowly in the plane of the laser focus for fresh exposure of the sample. Additionally, all experiments were carried out in a dry argon atmosphere to protect the sample from atmospheric moisture and oxygen. The purity of 7-AI was checked by mass spectrometry and high-performance liquid chromatography (HPLC). No evidence of impurity was found.

E. Synthesis of the N-deuterated 7-AI and 7-MeAI. A major and serious problem in the study of the deuterated species in solution is the exchange of deuterium with residual water in the environment (moisture in solvent, optical cell etc.). Thus, a relatively low N-deuterated 7-AI is not a problem in mass spectrometric studies as the femtosecond dynamics can be carried out solely for the selected species. In solution it is important to achieve high exchange yields because the measurement involves bulk species. The following new procedure for 7-AI offered an exchange yield of ~95% or higher.

The conversion of 7-AI into its N′-deuterated derivative *d*-7-AI was carried out under an atmosphere of dry argon using Schlenk tubes and glassware that was flame dried with a Bunsen burner prior to use. In a typical procedure, a solution of 1.0 g (8.71 mmol) of 7-AI in 40 mL of ether was treated slowly with 320 mg (13.3 mmol) of sodium hydride. After the resulting suspension was stirred for 2.5 h at room temperature under slightly reduced pressure, 5 mL (250 mmol) of deuterium oxide

(isotopic purity 99.9%) was added. The organic layer was separated, washed once with 3 mL of deuterium oxide, and dried over anhydrous magnesium sulfate. The colorless supernatant was filtered and the filtrate was concentrated to ca. 4 mL in vacuo. After the concentrate was cooled to 0 °C, colorless crystals precipitated which were filtered and dried in vacuo. The ^{1}H NMR spectral analysis (300 MHz, $CDCl_3$) revealed an isotopic purity of ~95%.

The sample 7-MeAI (7-methyl-7*H*-pyrrolo[2,3-*b*]pyridine) was obtained and purified as described before.[26] The purity was checked by TLC and ^{1}H NMR spectroscopy.

F. Treatment of Data. The femtosecond transients were analyzed using a least-squares fitting program. To account for the finite experimental response, the exponential decay terms were convoluted with a Gaussian response function $g(\tau)$. The resulting time-dependent signal $S(t)$ is given by

$$S(t) = \sum_i c_i \int_{-\infty}^{t} g(\tau) \exp[(t-\tau)/\tau_i]\, dt \qquad (1)$$

which can be solved analytically to give

$$S(t) = \sum_i c_i \sigma \exp\left[\left(\frac{\sigma}{2\tau_i}\right)^2 - \frac{t}{\tau_i}\right]\left(1 - \mathrm{erf}\left(\frac{\sigma}{2\tau_i} - \frac{t}{\sigma}\right)\right) \qquad (2)$$

where c_i is the amplitude of the component with decay time τ_i and σ is related to the fwhm of the excitation pulse (σ = fwhm/1.6651). Equation 2 was used to analyze both the decay (positive c_i) and the rise (negative c_i) components. The quality of the fits were judged using the χ^2 criteria.

III. Results

A. Steady-State Spectra: Absorption and Fluorescence. All experiments were carried out for a 7-AI sample concentration of c_0 = 20 mM, corresponding to an actual dimer concentration [D] of 8.9 mM. The ratio of the dimer to monomer concentration is 4 because the association constant in 3-methylpentane at room temperature is $K = 1800\ M^{-1}$;[7] for 2M ↔ D one can calculate [D] from $K = [D]/(c_0 - 2[D])^2$. Since both the dimer and the monomer absorb in the same wavelength region, the absorption band between 250 and 320 nm (Figure 2a) is a superposition of the two species. However, since the dimer absorption is more red-shifted, the dimer can be predominantly excited at 320 nm.[7] The fluorescence spectrum of 7-AI exhibits two broad and structureless emission bands. The strong band extends from 420 to about 600 nm, in nonpolar solvents and has a maximum at 480 nm. It has been shown to arise from the tautomer.[5,6] The second band, extending from 290 nm and up to ~430 nm, is mainly due to emission from the 7-AI monomer, on the nanosecond time scale.

Figure 2b shows the absorption and emission spectra of 7-MeAI—see Scheme 2. In contrast to 7-AI, there is a broad absorption band around 380 nm which corresponds to the $S_1 \leftarrow S_0$ transition. The fluorescence, however, is similar to the *tautomer* fluorescence of the 7-AI dimer.[6] It is worth noting that there is a large Stokes shift between the absorption and the emission in 7-AI, indicating a substantial molecular reorganization due to proton transfer. As discussed below, the tautomer molecular structure and excitation are distinct from that of the monomer; for 7-AI, the hydrogen is on the pyrrolic nitrogen (five-membered ring) while in the tautomer it is on the pyridine nitrogen (six-membered ring).

B. Femtosecond Time-Resolved Absorption. In Figure 3, we show the transient absorption of 7-AI at different probe wavelengths with excitation at 320 nm in 3-methylpentane. All transients are dominated by the excited-state absorption (positive absorbance) and not the stimulated emission. The transient absorption decays with the following general components: $\tau = 1.2 \pm 0.4$ ps, a slower $\tau' = 15 \pm 5$ ps; any residual signal represents a background of the nanosecond decay component. For all transients of the different wavelengths we used the same τ and τ' but varied the amplitudes. The amplitude of the 1 ps

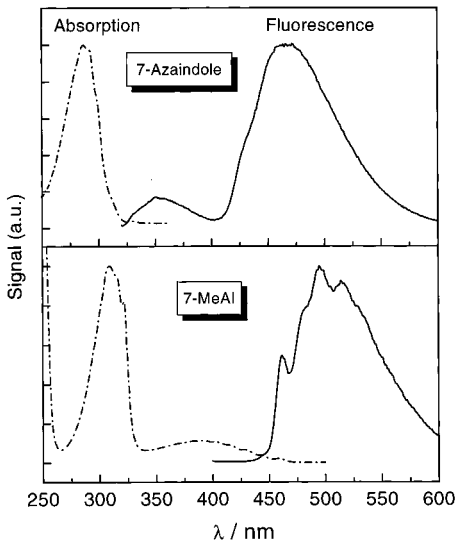

Figure 2. Steady-state absorption and fluorescence spectra (excitation at 320 nm) of (a) 7-AI (2×10^{-2} M) and (b) 7-MeAI (10^{-4} M) in 3-methylpentane.

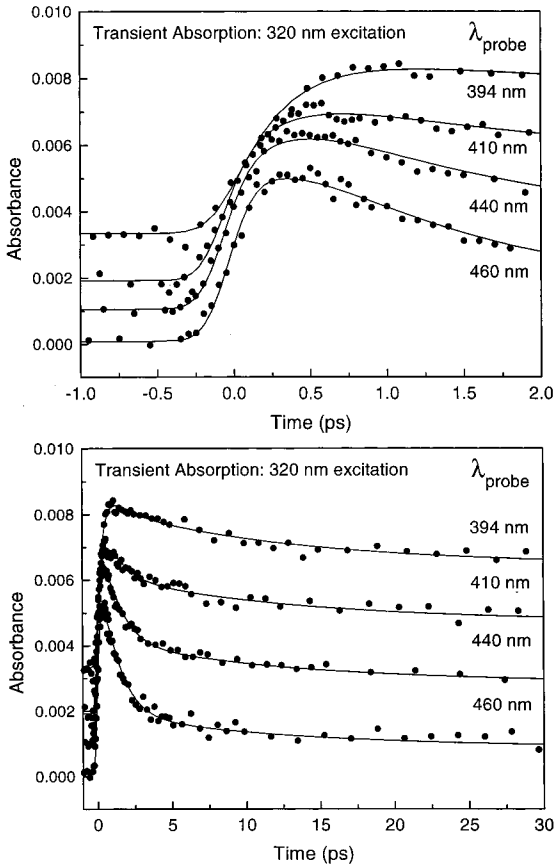

Figure 3. Femtosecond transient absorption of the 7-AI dimer in 3-methylpentane, probed at four different wavelengths. The excitation was at 320 nm. Upper panel: short time range, lower panel: long time range.

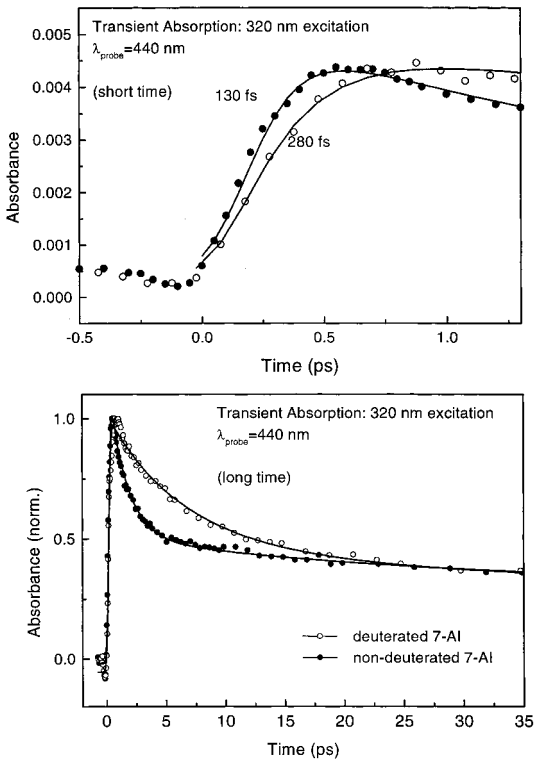

Figure 4. Effect of deuterium substitution on the transient absorption of the 7-AI dimer in 3-methylpentane, probed at 440 nm. The excitation was at 320 nm. Upper panel: short time range, lower panel: long time range.

decay component is larger at longer probe wavelengths and vanishes at 394 nm. In contrast, the amplitude of the 15 ps component is relatively constant over the range of the probe wavelengths used. The absorption at 394 nm exhibits a rise of 350 fs, while at longer probe wavelength the rise is within our time resolution. The above analysis is made independent of a model and simply according to a function which, with time, rises and decays (with τ and τ' and the nanosecond component).

The effect of isotopic substitution on the transient absorption dynamics at 440 nm is demonstrated in Figure 4. It is evident that both the rise time of the absorption and the subsequent decay time are significantly lengthened by the deuteration; the analysis of the data in terms of the exponential rise and exponential decay yields a rise time of 280 $\pm$ 100 fs for the deuterated species compared to 130 fs rise (limited by response) in nondeuterated 7-AI. The decay time τ changes from 1.2 ps to $\sim$ 5.0 ps; the larger time constant τ' appears in the figure to be similar.

To investigate the role of the excited state dynamics of the tautomer we measured the transient absorption of the tautomer model compound, 7-MeAI, excited at 320 nm (Figure 5): The analysis of the data indicates that the transient absorption rises within our time resolution and then decays with approximately 25 ps time constant. There is also a residual background. Recall that the lifetime of the tautomer is 3.2 ns.[8] Clearly, the transient absorption does not exhibit a major ultrashort decay component as observed in the 7-AI dimer.

C. Femtosecond Time-Resolved Fluorescence. Figure 6 shows the fluorescence transients of 7-AI in *n*-hexadecane at three different emission wavelengths with the excitation at 266 nm. For 360 nm detection (Figure 6a), we obtained a decay with a 1 ps time constant. For 480 nm detection, we observed a biexponential rise (Figure 6c). The short-time component of the rise is $\sim$1 ps and the long-time component is $\sim$12 ps. As

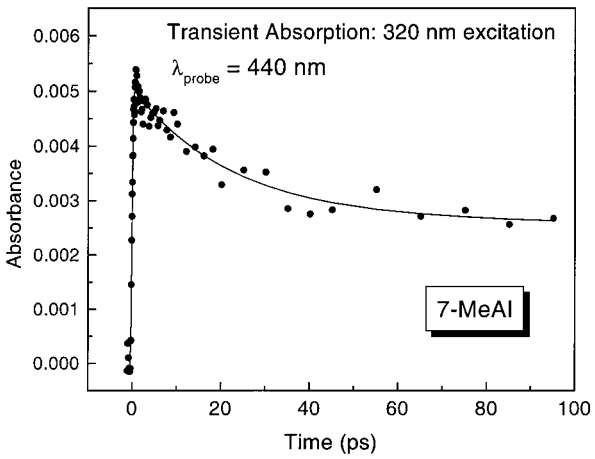

Figure 5. Transient absorption of 7-MeAI in 3-methylpentane (10^{-4} M), probed at 440 nm. The excitation was at 320 nm.

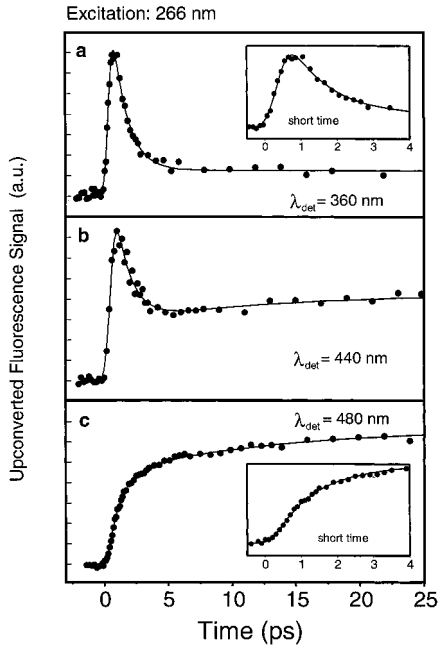

Figure 6. Femtosecond fluorescence transients of 7-AI in *n*-hexadecane, for three different detection wavelengths. The insets show an enlargement of the short time range. The excitation was at 266 nm.

shown later, a smaller femtosecond component could also be present. When the detection was at 440 nm, the observed transients give the apparent superposition of the signals at 360 and 480 nm.

The effect of isotopic substitution was also studied. The deuterated 7-AI (*d*-7-AI) was investigated under the same conditions. The fluorescence at 360 nm is substantially influenced by the deuteration: the time constant changes from 1 to 5 ps. In contrast, the rise of the tautomer fluorescence shows an apparent less of a change: as shown in Figure 7, the 1 ps component changes to 1.4 ps upon deuteration, whereas no significant change in the 12 ps time constant could be observed. However, as discussed below the deuteration is critical both in terms of the real concentration of *d*-7-AI dimers in the sample and the dynamics. Finally, a comparison of the transient behavior at two different excitation wavelengths is made in Figure 8. Upon decreasing the excitation energy (from 266 to 310 nm) the amplitude of the 12 ps component decreases. In what follows, we shall refer to a 1 and 10 ps component without giving the actual values simply to signify the time scale.

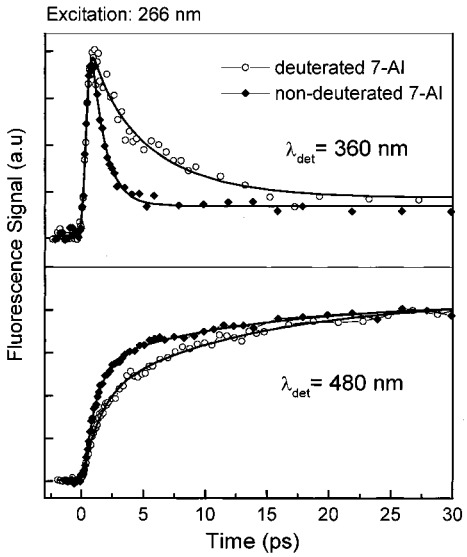

Figure 7. Effect of deuterium substitution on the femtosecond-fluorescence transients of 7-AI in hexadecane, detected at 360 and 480 nm. The excitation was at 266 nm. Results for both 7-AI and *d*-7-AI are shown.

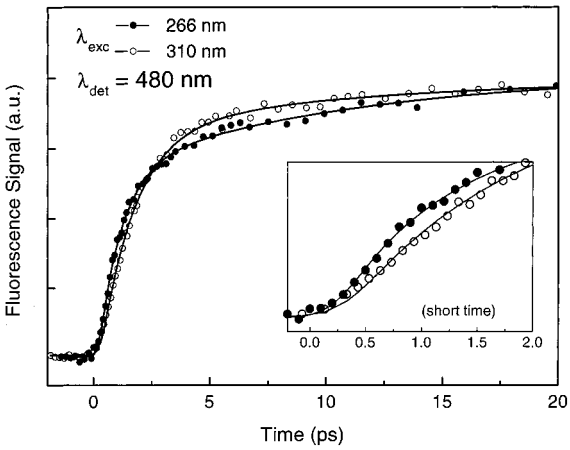

Figure 8. Effect of the excitation energy on the femtosecond-fluorescence transients of 7-AI in hexadecane, detected at 480 nm. The insets show an enlargement of the short time range.

IV. Discussion

A. Time Scales of Proton Transfer. We have four observations which are critical for the elucidation of the dynamics of proton transfer. These are (1) the temporal behavior of the observed transient absorption; (2) the temporal behavior observed in the build up of the tautomer emission; (3) the dramatic isotope effect; and (4) the rise of the initial signal. In transient absorption following excitation at the lowest energy (320 nm) near the 0,0 transition (Figure 2) we observe the 1 ps decay and the 10 ps decay (Figure 3). The tautomer emission at 480 nm similarly rises with the two distinct time constants, 1 ps and the 10 ps (Figure 6); the fluorescence at 360 nm decays with the 1-ps component but with no 10-ps component present. (The actual signal amplitude at 480 nm is much larger than that at 360 nm.) The isotope effect of the initial decay for 360 nm emission detection (1 vs 5 ps, Figure 7) and similarly for the transient absorption (1 vs 5 ps, Figure 4) is striking.

The above results indicate that both the femtosecond transient absorption and fluorescence show manifestation of proton transfer and "tunneling" and that the transfer is complete on the time scale of picosecond. The long decay component, being less sensitive to the isotope substitution, reflects solvation/vibrational cooling following the transfer, as discussed below. The key question then is the following: what is the time scale for the transfer of the *first* proton? We have examined very carefully the rise of the transient absorption, which must reflect the dynamics of the initial state(s) of the system, and observed the isotope effect shown in Figure 4. If the signal is due to the initial dimer we expect no isotope effect on the rise time and both transients should rise within our time resolution. Accordingly, the first proton transfer occurs in 280 fs (*d*-7-AI), in the small-barrier regime. Note that we excite at 320 nm with no significant excess energy (other than thermal) and any dynamics must involve a barrier if present. Excitation at higher energy increases the "above-the-barrier" crossing, as discussed below.

B. The Tautomerization Model. Guided by the above results, we first give a phenomenological kinetic description of the processes, keeping in mind that the actual landscape of the potential energy surface (PES) is multidimensional and that different trajectories must be considered; in subsection C, we discuss the nuclear dynamics.

After preparation of the system near the bottom of the excited pair potential, the first transfer, leading to the intermediate structure I, whose identity will be discussed below, occurs on the fs time scale (k_1). Subsequently, the second proton moves on a 1 ps time scale (k_2), forming the final tautomeric structure. However, this structure ($T^\dagger$) is vibrationally (and perhaps even electronically) excited in a nonequilibrated state. The relaxation process takes place within tens of picoseconds. If the initial excitation is much above the barrier, then in addition to the two steps involving the intermediate we expect that the transfer from the pair to the tautomer (k) becomes significant. When the excess energy becomes much above the barrier, the reaction will exhibit barrierless rates unless vibrational relaxation is very efficient to bring the system to lower energies.

In actuality, a family of trajectories are made possible for the reaction with the partition between I and T determined by the barrier height(s) of P to T and by the lifetime of I.[27] Thus, our scheme is the following:

$$P \xrightarrow{k_1} I \xrightarrow{k_2} T^\dagger \quad (1)$$

$$P \xrightarrow{k} T^\dagger \quad (2)$$

This concept was emphasized in refs 17 and 27 and is crucial to many complex reactions.[28] The solution of the kinetic equations (1) and (2) is straightforward. In Figure 9 we display the population changes with time for P, I, and $T^\dagger$ when $k_1^{-1} =$ 250 fs, $k_2^{-1} = 1$ ps, and the relaxation of the hot $T^\dagger$ is 10 ps in eq 1. The purpose of this figure is to illustrate the consequences of femtosecond rearrangement and relaxation on the transfer for the first proton and the overwhelming population of T at longer times. Hence, it is critical to resolve the early dynamics with proper femtosecond resolution and to examine the isotope effect and any rise on such time scales. Clearly, the steady-state emission will be dominated by the T emission.

The tautomer must be formed in a distribution of vibrational energies since its electronic energy is below that of the initial pair. Hence, we consider the relaxation of the distribution following the transfer. Here, to simplify, two types of T are considered kinetically, those with essentially no vibrational energy (T_c) and those which are vibrationally hot (T_h). The T_c species will decay with the normal nanosecond lifetime of T, while T_h will decay on the picosecond time scale. The change of the transient absorption with the probe wavelength is very

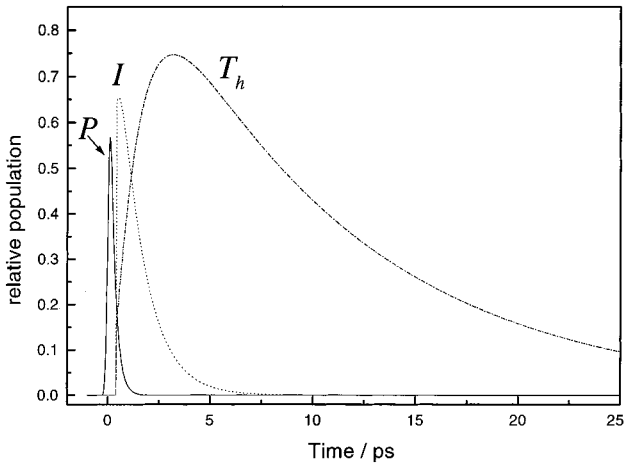

Figure 9. Simulation of the time-dependent populations of P, I, and T_h for the consecutive reaction scheme: $P \rightarrow I \rightarrow T_h$, taking the lifetime of 10 ps for T_h, as discussed in the text for one of two prominent channels. Note the importance of detecting with real femtosecond resolution (for D and I), the overwhelming emission T_h, and the appearance of the rise as multiple exponentials, including a 250 fs component.

indicative of *the probing along the reaction coordinate*. To quantify this trend of probing the different populations of P, I, T_h, and T_c, we solved eq 1 considering that I produces T_h and T_c, with the following total signal: $S(t) = \sigma_I N_I(t) + \sigma_{Th} N_{Th}(t) + \sigma_{Tc} N_{Tc}(t)$, where $N(t)$ is the population and σ is the relative cross section for absorption. Fitting the data in Figure 3 to this scheme, we obtained the following results which agree well with the clearly observed trend of the data.

Starting with the transient absorption for 320 nm *pump* and 460 nm *probe* the pronounced decay (1.2 ps) of I, which is formed in 280 fs for the deuterated species and somewhat less for the nondeuterated 7-AI, is dominant. Upon probing at shorter wavelengths, the tautomer contribution becomes stronger which is evidenced from the decrease of the 1 ps decay component in the transient and the increase of the amplitude of the longer decay component. It is interesting to note that measurements of the (transient) tautomer absorption spectrum in the electronic ground state[10] showed a maximum at about 380 nm. This is consistent with the tautomer-type absorption found in 7-MeAI (see Figure 2). Assuming that the excitation remains localized on only *one* 7-AI moiety in the pair, as shown theoretically,[21,22] the excited tautomer state is expected to have similar absorption properties as the monomeric tautomer in the ground state since one member of the pair can be viewed as being in its electronic ground state. Finally, at 394 nm the decay of the intermediate and the rise of the tautomer cancel each other almost completely (Figure 3). With the same model we obtained the effective cross sections for the four probe wavelengths studied: At 394 nm, $R = \sigma_T$ (total)$/\sigma_I = 1.8$; 410 nm, $R = 1.2$, 440 nm, $R = 0.8$; and at 460 nm, $R = 0.4$, reflecting a factor of 4.5 change in the ratio (see Figure 3). Accordingly, in the blue side of probing we are detecting preferentially the tautomer, T_h and T_c, and in the red side of probing we observe more of the I species. The 10−15 ps component thus is a measure of the vibrational cooling of T_h, which leads to sharpening of the hot spectrum.[24] On the other hand, the nanosecond background is due to the T_c population decaying with 3.2 ns.

The fact that the fluorescence upconversion signal at 360 nm (Figure 6) decays with a 1 ps time supports the above picture with this emission originating from the intermediate state on this time scale. A large transition dipole moment, obtained by our ab initio calculations between S_1 and S_0 state of the intermediate, further supports this interpretation. As in transient absorption, it is expected that the I emission rises with the rate k_1 for 7-AI and $(280\ \text{fs})^{-1}$ for *d*-7-AI), but we were not able to resolve this rise due to the lesser time resolution of the upconversion method and the weak fluorescence signal at 360 nm. Because of its better time resolution, transient absorption experiments at 440 nm on the highly deuterium-enriched 7-AI sample (>90%) enabled us to directly monitor this rise and provided the time scale of ∼280 fs. By detecting the emission at 480 nm we directly observe the formation of the tautomer ($(1\ \text{ps})^{-1}$, k_2) followed by the relaxation process of $\sim(10\ \text{ps})^{-1}$ as discussed above. Note that the emission at 440 nm is also a superposition of the two species, consistent with the transient absorption picture.

C. Dynamics. First, we consider the preparation of the system at or near the zero-point energy (ZPE) of the pair. This is typical for the transient absorption with excitation at 320 nm. With the equivalence of the two hydrogen bonds in the static structure of the pair it is interesting to consider the nature of the process that leads to the structural changes. Because the time scale of the proton motion is observed to be relatively short, compared to the energy redistribution, the reaction center involves primarily the N−H and N···N intermolecular motions. The time scale of the proton motion, however, is longer than (or comparable to) the changes in the electronic distribution on excitation and the nuclear vibrational motions of the N−H and N···N stretches. This last inequality allows for the asymmetric motion of one of the protons, and, because one moiety is excited, the proton ultimately transfers, leading to the I. The N···N stretch is about 120 cm^{-1} and the N−H stretch is about 2800 cm^{-1}, giving 280 and 12 fs, respectively. Therefore, on the time scale of 0.2−1 ps (typical reaction times) the "asymmetric reaction coordinate" for the two particles is established.

In the isolated pair (molecular beam experiments) the evidence for the consecutive process comes from three independent measurements: (i) the biexponential decays observed by femtosecond-resolved mass spectrometry at different vibrational energies (indicating near zero value) and for different isotopic composition of the reactive hydrogens, labeled HH, HD, DD;[17] (ii) the rise and decay observed by femtosecond-resolved Coulomb explosion[18] which arrested the intermediate and showed the corresponding two decays observed in ref 17 as rise and decay; (iii) the subpicosecond photoelectron spectra[19] of reactive and nonreactive dimers with the former having a lifetime of less than 1 ps, consistent with both femtosecond mass spectrometry and Coulomb explosion experiments. The results of ref 17 give different τ_1 (first transfer) and τ_2 (second transfer) for the vibrational energies (E) and isotopic composition: $\tau_1 =$ 360 fs $\tau_2 = 1.7$ ps ($E \sim 1$ kcal/mol); $\tau_1 = 650$ fs and $\tau_2 = 3.3$ ps ($E \sim 0$ kcal/mol); and $\tau_1 = 3$ ps and $\tau_2 = 25$ ps for ($E \sim 1$ kcal/mol), for the {ND, ND} species. At the same total energy of ∼1 kcal/mol, the {ND,NH} mass peak gives $\tau_1 = 1.5$ ps and $\tau_2 = 11$ ps, representing, remarkably, a close average for {NH,NH} and {ND,ND} constants. For the $E \sim 0$ case, the observed deuterium effect indicates the presence of tunneling and the isotope effect is the largest since these experiments were performed in a molecular beam with the average internal energy being less than about 10K. The ZPE of the N−H stretch is ∼1400 cm^{-1} while that of N···N is ∼60 cm^{-1}. Thus, in the simplified two-dimensional PES picture the barrier must be considered as the value above these ZPE up to the saddle point (see appendix), and its change as the N···N motion takes place. In other words, the N···N motion is critical in bringing about

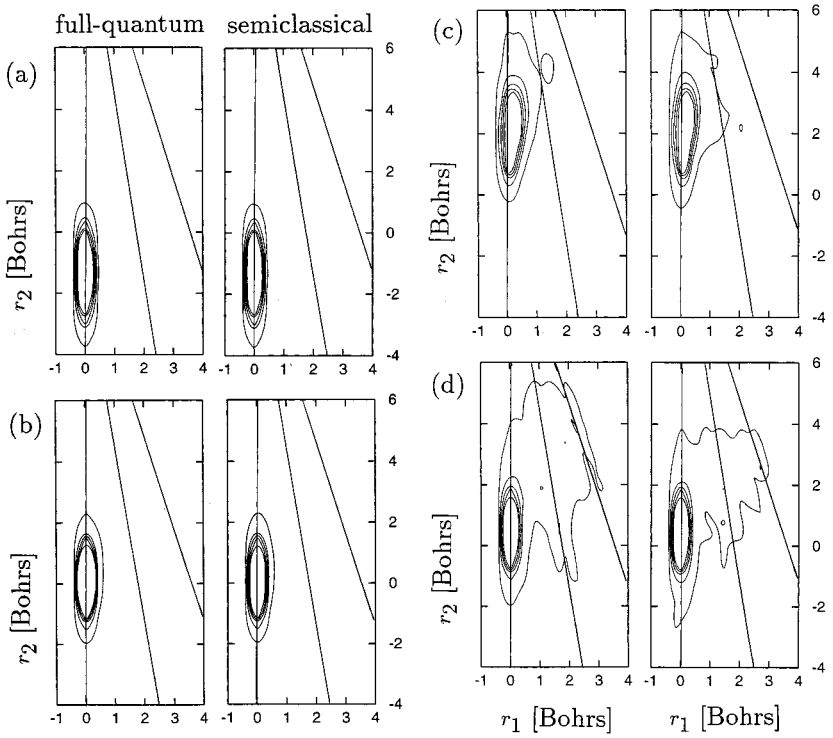

Figure 10. Adapted from ref 22 (see Acknowledgment): Comparison between the semiclassical and the full quantum mechanical wave packet, reduced to the space of reaction coordinates r_1 and r_2 (see text) at various different times after excitation: (a) 0 fs, (b) 48 fs, (c) 97 fs, (d) 164 fs. Wave packets are represented by five contour lines equally spaced by 0.045 units in the 0.005−0.185 range of amplitude. r_1 is the coordinate for the first proton transfer. The wave packet indeed visits this space on the ∼200 fs time scale (see text).

the transfer. In fact, in the gas phase[13] this mode is prominent in the excitation spectrum and is indeed a promoter of proton transfer. It is evident that, given the observed time scales, the multidimensionality (at least two dimensions) of the PES must be considered.[17]

Molecular dynamics calculations by Guallar, Batista, and Miller[22] indicate such effect of dimensionality. In Figure 10, we show their results for the motion of the wave packet initially localized on the femtosecond time scale and considering the reactive hydrogen displacement (r_1) and the N···N symmetric motion (r_2) among all modes. After the first 100 fs of nuclear motion in the N···N coordinate (relaxation) the *first* hydrogen moves in steps of ∼200 fs, entirely consistent with the experimental results. The authors point out the *dominance* of the consecutive two hydrogen motions, and the localization of the initial excitation on one monomer in the pair; the barrier for the concerted process was found to be located at higher energies. They also make the new assertion that the intermediate is more "covalent" in nature.

In nonpolar solvents, such as those used here, the barrier is expected to be similar to that for the gas-phase species. The solvent perturbation is in inducing vibrational relaxation and mediating intramolecular vibrational energy redistribution (IVR). Note that in the isolated molecule (microcanonical) there is no energy relaxation. Since the time scale of the transfer in the solution phase is hundreds of femtoseconds to 1 ps, we can neglect the effect of the solvent-induced relaxation when E is small and time scale femtoseconds to 1 ps. The major influence on this time scale is the room temperature initial *thermal energy* of the pair in the solvent. In other words, in solution the initial excitation carries with it enough thermal energy (in this case comparable to or larger than the barrier height) that the rates in solution have to be larger than those observed at low E in the gas phase. In fact, it is remarkable that the rate constants of $\tau_1 = 200$ fs and $\tau_2 = 1.6$ ps in the gas phase at $E = 1.5$ kcal/mol are similar to the ones reported here in nonpolar solvents ($\tau_1 = 280$ fs (DD), $\tau_1 \leq 130$ fs (HH), and $\tau_2 = 1.2$ ps (HH)). The 10 ps relaxation indeed reflects the role of the solvent-induced relaxation as the experiments on 7-MeAI (in the absence of proton transfer) demonstrated. The effect of thermal energy is very significant in view of the fact that the barrier is small and the N···N mode of 120 cm^{-1} accelerates the rate of proton transfer, as evidenced by the spectra in supersonic jets.[13] As a consequence of this thermal averaging, the isotope effect will be large but not as large as observed in the beam experiments.

In the condensed phase, excitation involving the N···N mode will be altered by the possible coupling to the solvent bath modes. If energy dissipates from the N···N motion to the solvent, then we expect a slowing down of the transfer. On the other hand, if the mode acquires energy from the bath, because of its low energy, the transfer may accelerate. The fluctuations will determine the net change of the rates. Another influence of the solvent is in the static perturbation of the potential energy, which may be different along the reaction path, especially in polar solvents. In the gas phase we have calculated the barrier height for the first transfer using the tunneling frequency expression (1D and 2D, barrier is ∼1.3 kcal/mol), indicating the effect of vibrational excess energy below and above the barrier.[17]

At higher excitation energies (e.g. 266 nm), the rise of the tautomer emission (480 nm) still shows the 1 and 10 ps components. The decay of the emission at 360 nm also shows the 1 ps component, with a large isotope effect of about a factor of 5. In the kinetics description discussed above, we quantified the analysis, considering the presence of all species HH, HD, and DH, and DD: the decay when fitted gives the 1 ps (28%) and 5 ps (78%) decay components, indicating that the sample contains some nondeuterated species (22%), consistent with isotopic enrichment of ∼80% on the monomer; (thus [DD] = 64%, [HD],[DH] = 32%, [HH] = 4%); note that for emission

measurements we used the old method of deuteration[25] but for transient absorption we used the new method (≥90% D). On the other hand, the apparent rise of emission at 480 nm is misleading, and when fitted properly we actually obtained similar results to the decay: 1 ps (28%) and 37% for the 5 ps and 35% for a 20 ps component. The 20 ps component does not show up on the decay since it is due to relaxation in the tautomer. Accordingly, both the femtosecond transient absorption and upconversion results are consistent with the general scheme outlined above. This isotope effect and the critical transient absorption measurements with high time resolution proved to be very important for the overall picture, and have not been examined before, as discussed below.

The wave packet launched in the pair at higher energies bifurcates into the I direction and the T direction. However, this bifurcation can be biased toward T by the many nonsynchronous trajectories which do not visit the I well.[27] In general, excitation above the barrier will form wave packets which contain two types of states, those with nonreactive modes $|n_1, n_2, ..., n_R = 0, n_R = 0, ..., n_j\rangle$ and those which contain the N−H and N···N modes $|n_1, n_2, ..., n_R \neq 0, n_R \neq 0, ..., n_j\rangle$. Thus, some population, after fast vibrational relaxation (VR), will proceed along the reactive coordinate(s) similar to the low-energy excitation while others may thermalize (IVR) and undergo barrier crossing. Any direct motion toward the tautomer, which must compete with vibrational relaxation, will appear asynchronous concerted as the process occurs at much higher energies above the barrier; entropically the synchronous concerted motion will be very unlikely.[27,28] It is interesting that a barrier crossing process at room temperature with a preexponential factor of $\sim 10^{13}$ s^{-1} will have a rate of $\sim$(1 ps)$^{-1}$ for a barrier of ∼1.5 kcal/mol. The fact that our experiments at 320 and 266 nm excitation give similar rates and isotope effect supports that the VR at these high energies is competitive.

D. Ab Initio Calculations of the PES. Various papers have been published on electronic structure calculations for the 7-AI monomer as well as the dimer (see refs 8, 20−22, 29−33). The dimer has been studied in its initial, intermediate, and tautomer states. However, there has been no attempt to scan the potential energy surface (PES) along the two proton coordinates, which is needed to elucidate the actual reaction coordinates for double proton transfer. As mentioned earlier, the work of Guallar et al.[22] provides the PES in the configuration space of the N···N and N−H motions.

A feasible method to calculate the energy and structure of excited states in molecular systems of the size of the 7-AI dimer (30 atoms) is the single excitation configuration interaction (CIS) approximation.[34] It is well-known that the method overestimates excitation energies due to insufficient treatment of electron correlation effects. Therefore, vertical excitation energies are often scaled to be comparable with experimental data. However, as far as relative energy changes on the excited-state PES are concerned, the method can provide valuable insights. Here, we report calculations of the PES for the pair. The calculations were carried out with Gaussian 94[35] at the CIS level using the 4-31G basis set. The completely optimized base pair structure in its lowest excited singlet state was used as a start geometry. The two proton coordinates were varied from 0.9 Å (initial) to 2.0 Å (tautomer) while all other internal coordinates were kept frozen; the equilibrium N−H bond distance in the pair is 1.0 Å. In total, 144 points were calculated on the excited-state potential energy surface.

Our ab initio calculations show that there are at least five excited-state crossings along the reaction coordinate which

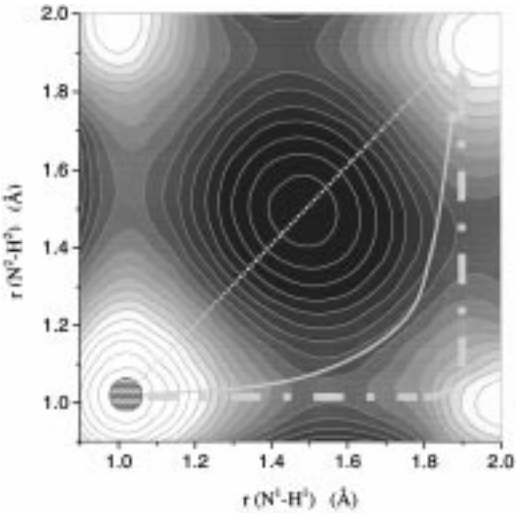

Figure 11. Contour plot of the two-dimensional potential energy surface obtained from our ab initio calculations at the CIS/4-31G level of theory (see text for details). The plot shows two extreme trajectories for the initial wave packet: the fully synchronous, diagonal pathway for concerted double proton transfer (dotted) and the consecutive pathway via the intermediate well (dash-dot). We also show the family of asynchronous motion (see ref 27).

makes a simplified discussion about the involvement of specific states very difficult. Thus, the actual electronic pathway from the pair to the tautomer state depends on the coupling between these electronic states. On the basis of the assumption that there is strong coupling between low-lying states, we have calculated the *adiabatic* two-dimensional PES for the pair along the two proton coordinates; i.e., we consider always the lowest excited singlet state for each nuclear configuration.

Figure 11 shows a contour plot of the calculated two-dimensional PES. The calculation implicates that a *synchronous (diagonal) motion* along both coordinates is associated with a substantial energy barrier compared with relatively low-energy barriers for the sequential process(es). Hence, these results support the nonconcerted mechanism, as do the reported experiments on isolated reactions, here in nonpolar solvents, and by recent theoretical calculations[22] at the CIS/6-31G level of theory. Furthermore, it is worth noting that the excited-state energies of the initial base pair and the final tautomer configuration without nuclear−electronic reorganization involving all other coordinates are similar (within 0.3 eV); the net asymmetry of the potentials for the initial and final states occurs as a result of the reorganization.

To test the reliability of the computational method used we also calculated the one-dimensional PES along a single N^1−H···N^1 bond (i.e. the first step of proton transfer) for different N^1···N^1 distances in order to study the influence of the heavy-atom distance change on the reaction barrier. In this calculation *all* other internal coordinates have been varied freely. As shown in Figure 12 the barrier is reduced by 60% if the N···N distance changes from 2.93 to 2.73 Å. These results are in qualitative agreement with theoretical models for single proton-transfer reactions.[36]

E. Conclusion and Comparison with Other Work. The isolated pair dynamics are understood from the experimental and theoretical studies. Three different experimental approaches of time resolution have given consistent results regarding the time scales and the consecutive dynamics of the transfer: femtosecond-resolved mass spectrometry[17] shows the exponential decays of P, I, and T; femtosecond-resolved Coulomb explosion[18] shows a rise and decay for the intermediate I; and

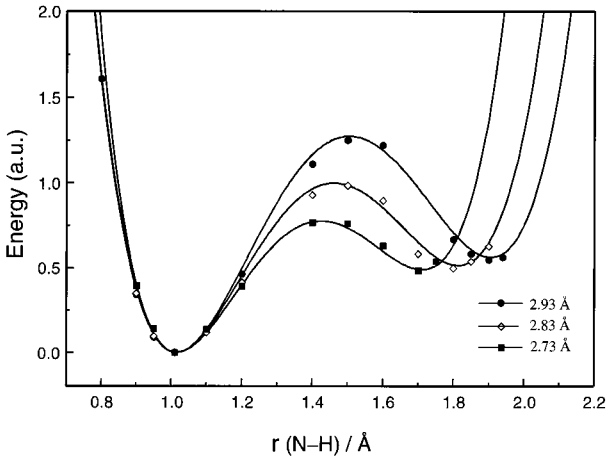

Figure 12. One-dimensional potential energy surface for the first transfer in the 7-AI dimer computed for different N···N distances (see text for details). Note the lowering of the barrier as the N···N distance decreases.

subpicosecond photoelectron study[19] shows that the excited state lifetime of the pair is substantially less than a picosecond. As pointed out earlier,[17] the observed femtosecond decay of the pair is also entirely consistent with the spectral broadening reported[13] for the reactive pair in supersonic jets, especially when the N···N (120 cm^{-1}) mode is involved; nonreactive pairs were also studied[13,14,19] with the suggestion of a T-shaped geometry.

Theoretically, the reported ab initio studies are consistent with this picture. From the dynamics point of view, two studies at the CIS level of theory, that of ref 22 and the results reported here, indicate the two-step mechanism with the barrier for the synchronous, concerted motion being higher in energy. Moreover, the molecular dynamics[22] picture elucidate the motion of the wave packet in the N···N and N−H coordinates and give time scales for the nuclear relaxation ($\leq$100 fs) and for the first proton transfer (200 fs steps). The excitation was shown to be mainly localized on one moiety and that the intermediate is mostly covalent in nature (proton vs hydrogen atom transfer; proton/electron transfer). It was emphasized earlier that the one-dimensional picture of proton transfer is inappropriate and that the dynamics of concerted and nonconcerted motions are the consequences of the symmetric and the asymmetric nuclear vibrations.[17] The MD simulation is entirely consistent with this reduced 2D picture, as IVR to other modes is on a longer time scale. Finally, the initial femtosecond excitation forms a localized wave packet in the nuclear coordinate space, and this localization is associated with electronic charge redistribution from the five- to the six-membered ring.

In the gas phase, the isotope effect and energy dependence[17] are in agreement with a barrier reaction involving tunneling, observed also at near 0 kcal/mol of excess vibrational energy (see Appendix). The barrier for the first transfer is estimated to be ~1.3 kcal/mol (~500 cm^{-1}) and for the second step, from the isotope effect to be at least 2.6 kcal/mol. In the jet spectra,[13] the N···N bond narrows upon deuteration, consistent with the trend observed in the rates, but because the lines are inhomogeneously broadened they do not reflect the actual change in the dynamics. Following the femtosecond wave packet excitation, the nuclear relaxation with motion in the N···N coordinate will bring the proton closer to the nitrogen and on this time scale the asymmetric motion leads to the first proton transfer. According to the results of Guallar et al.[22] this first transfer is accompanied by electron transfer between the two monomers, and thus the dominance of a covalent (biradical-type) intermediate; the zwitterion intermediate will come in at shorter N···N distances.

In nonpolar solvents the isolated pair picture is a basic one. We resolve a 130 fs (HH), 280 fs (DD) rise for the first transfer and close to 1 ps (HH) and 5ps (DD) for the second one. These reaction times in 3-methylpentane and in *n*-hexadecane are remarkably close to those observed in the isolated pair (molecular beam) when the vibrational energy exceeds the barrier height. For example, when the excess energy was 1.5 kcal/mol, the observed decay time constants were 200 fs and 1.6 ps. The key point here is that on these ultrashort time scales the energy dissipation to the solvent or by the solvent is only significant when the molecule in solution is excited at high energies. Thus, at low energies (such as in our experiment near the 0,0 transition at 320 nm), the solvent effect is a room temperature thermal excitation. In such molecules as 7-AI pair, the thermal energy is significant when compared with the barrier height and it is therefore reasonable to predict those rates based on "above-the-barrier" gas-phase (molecular beam) values, of course with proper thermal averaging. This problem is reminiscent of stilbene isomerization with a barrier of ~3 kcal/mol.[37] The isotope effect in solution should be less than in the beam experiment because of the thermal averaging and the fact that in such cases the isotope effect could be dominated by "above-the-barrier" to "below-the-barrier" energy lowering.[38] Solvent-induced vibrational relaxation in the tautomer (spectral narrowing) is observed on the tens of picoseconds, consistent with the results of Tahara et al.;[24] earlier,[25] we interpreted this component differently because of the lack of time resolution to observe the first step.

Our observed isotope effect in solution is different from that observed by Tahara et al.[24] Furthermore, their excitation wavelength was at 270 nm, much above the zero-point energy. The authors reported a small component of ~200 fs and relate it to the idea of exciting the L_b state followed by relaxation into the lower-energy L_a state from which the proton transfer occurs concertedly. The observed *similarity* of the isotope effect on the fluorescence (380 nm) decay and fluorescence (540 nm) rise made them suggest a 200 fs L_b/L_a conversion and 1 ps concerted, double-proton transfer. We have some points to make. First, all their experiments were made using fluorescence upconversion with time resolution less than that of the transient absorption reported here and it is difficult to probe along the reaction coordinate without both types of experiments as shown here.

Second, it its important to realize that the isotopic enrichment in bulk solutions is a nontrivial task as for 7-AI there is exchange of D with water from the environment; this is not a problem for the studies made using mass spectrometry, as discussed above. We had to develop a new way of obtaining high enrichment and indeed when we reached the 90% (or even higher) we observed a clean isotope effect on the rates. A sample of 60% enrichment will give a misleading apparent rise (or decay) dominated by contributions from three species (HH, HD/DH, and DD pairs), as discussed in the text. Third, the issue of L_b and L_a interconversion is inconsistent with the results of Guallar et al.[22] who found that the oscillator strength to the ground state for the L_a is much larger than that of the L_b state, with the excitation being monomer type. This is consistent with our ab initio calculation at the CIS level. Because of the fact that the authors excited the pair at 270 nm, the relatively small 200 fs component could be explained as due to VR/IVR in the pair, similar to our 266 nm excitation at energies much above

the barrier and where the wave packet is composed of reactive and nonreactive modes. Note that relaxations in the initial pair are different from those of the tautomer; the former is reactive and has a barrier, i.e., many continuum states are available (fs relaxation) while the latter cools only by VR/IVR.

Our picture in the condensed phase is consistent with work on the picosecond time scale.[15] At room temperature they observed the rise of the tautomer emission (480 nm) within ~5 ps, not resolved. However, as they lowered the temperature to 77 K they observed an additional much slower rise which they attributed to the "cold" distribution of molecules made possible by VR; excitation was at 263.5 nm. The emission spectra at low temperature for different excitation wavelength gave a barrier of ~700 cm^{-1}. Share et al.[16] reported an excited-state reaction time of 1.4 ps (HH) and 4 ps (DD) with a time resolution of 0.3 ps. This isotope effect is also consistent with our factor of ~5 observed in transient absorption and emission, but *not* in agreement with the results reported in ref 24. The reported transient absorption of Share et al. showed a rise within their pulse with no decay at longer times (up to 6 ps). This was attributed to a decay channel into the ground state of the tautomer. Near this wavelength of probing (375 nm) we have shown that the transient absorption is composed of two contributions, that of the intermediate and the tautomer, and in fact this addition leads to a cancellation which results in an observed transient very similar to the one we present in Figure 3. As discussed above, from theory, the tautomer excited species is expected to have one of the moieties in the ground state, and thus has similar absorption; the ground-state tautomer absorbs at ~380 nm, as confirmed by studies on the microsecond time scale and by the absorption of model tautomer 7-MeAI (Figure 2).

Ingham and El-Bayoumi,[7] in a thorough study, have shown that the fluorescence of the tautomer (F_2) to that of the initial population (F_1) changes with temperature. At steady state this ratio of F_2/F_1 was related to an Arrhenius activation yielding a barrier of 1.4 kcal/mol, in excellent agreement with the value obtained from the tunneling times measured in the molecular beam experiments.[17] Furthermore, the F_2/F_1 ratio does not vanish at low temperature, supporting the tunneling mechanism. The effect of deuterium substitution (see refs 17 and 39) is not as large as observed in the beam experiment (see Appendix). As discussed in the text, the full isotope effect of tunneling can only be observed if the thermal averaging is minimum. Naturally, the steady-state measurements, because of the lack of time resolution, could not distinguish between population in the pair and in the intermediate state nor could they obtain the time scale for the double proton transfer process. However, the temperature dependence of these steady-state fluorescence experiments and the study of 7-MeAI by Ingham and El-Bayoumi provided a real base for all subsequent work. Our efforts on real time dynamics of proton transfer here and elsewhere provide a unified picture which may prove applicable to the dynamics in many other systems of proton and hydrogen atom transfers.[40−43]

In conclusion, the big picture of double proton transfer is clear: both protons (hydrogens) are transferred on a 1 ps time scale when the internal energy is near (or above) the barrier height value. Only when the internal energy is low (beam and low-temperature experiments) can we examine the processes of tunneling and nonconcertedness. Two cautionary remarks are worth mentioning. First, for a low-barrier reaction,[37,44] the influence of the thermal energy in solutions is significant, and this averaging will reduce the apparent isotope effect and make fuzzy the distinction for different trajectories. Second, for systems undergoing proton transfer, with mixed covalent and ionic characters along the reaction path, the comparison between theory (of PES) and experiment is valid only in the isolated molecule; in the solvent, the energy of the transition state or the potential minima could be altered and the comparison becomes ill-defined. Furthermore, as pointed out by Roos,[45] the state of theoretical computations is near-rigorous for ground-state potentials, but less so for excited-state potentials. Hence, the comparison should be made with this fact in mind. Finally, the branching of trajectories[27,28] is general in isolated elementary and complex reactions, including proton transfer,[46] and the time scale of solvation dynamics, relative to those of the intramolecular motions of the light and heavy atoms, is what determines the elementary description in the condensed phase; the two regimes involving intramolecular transfer with solvent reorganization or transfer along a global solvent coordinate.[47]

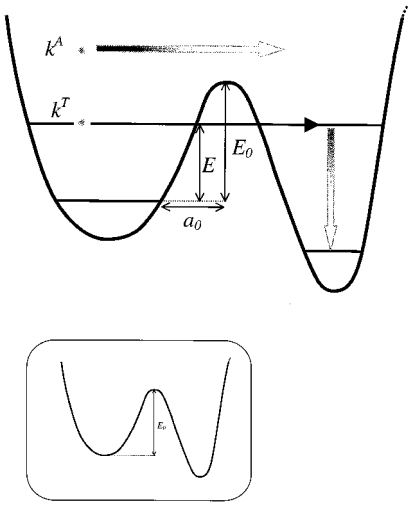

Figure 13. A schematic defining the tunneling (k^T) and barrier crossing (k^A) rates and parameters. E is the available energy above the ZPE, E_0 is the barrier height measured above the ZPE, and a_0 is half of the width of the barrier parabola. k^T is given in the Appendix and k^A is the standard Arrhenius expression. Note that the inset represents the picture drawn in many publications (classical limit) and is only valid if $E_0 \gg$ ZPE.

Acknowledgment. This work was supported by the National Science Foundation. T.F. is grateful for financial support from the Deutsche Forschungsgemeinschaft. M.C. thanks the Swedish Foundation for International Cooperation in Research and Higher Education (STINT) for its generous fellowship. We thank Dr. W. Kühnle for his help with HPLC. We also acknowledge computing time from the Gesellschaft für wissenschaftliche Datenverarbeitung (GWDG) in Göttingen, Germany, and helpful discussion with Dr. Klaus B. Møller. We thank Dr. Victor S. Batista for sending us the referenced manuscript and Figure 10 prior to publication and for useful discussion.

Appendix. Tunneling Rates and the Effect of ZPE

In Figure 13, the key parameters are defined for tunneling and (above) barrier crossing rates. A point that has been overlooked is the classical limit. In many publications, the barrier height is considered from the bottom of the well to the top of the barrier. The tunneling frequency (rate, when the asymmetry of the potential induces irreversibility[48]) is calculated according to the expression:

$$k^T = \nu \exp\left[-\frac{\pi a_0}{\hbar}\sqrt{2m(E_0 - E)}\right] \qquad \text{(A1)}$$

where ν is the reaction-coordinate frequency (N−H mode), a_0 is the half-width of the energy barrier and E_0 is its height, E is the available energy above the ZPE, and m is the effective mass of the particle. In the case where E_0 is very large compared to the ZPE, one may justify the neglect of the ZPE and an expression for the isotope effect may be written,[7] considering only the change of the frequency (NH/ND) and the mass of the particle (H/D). However, for the 7-AI system, the ZPE of the N−H coordinate is ∼1400 cm^{-1} and the E_0 value is ∼500 cm^{-1}. Accordingly, E_0 is the value above the ZPE (to the top of the barrier) and upon replacing H by D, the isotope effect will manifest itself not only in the mass change but also in the new value of E_0 (measured from the ZPE of now ∼1000 cm^{-1}) and the increased distance (a_0 = 0.36 Å) over which tunneling occurs.

For the 7-AI system, we calculated the rate and the isotope effect using the above equation: for E_0 = 500 cm^{-1}, a_0^{H} = 0.27 Å,[7,39] ν_{N-H} = 2800 cm^{-1}, and m_{H} = 1, we obtained:

$$k_{\mathrm{H}}{}^{-1}(E = 0) \approx 0.6 \text{ ps}$$

$$k_{\mathrm{H}}{}^{-1}(E \sim 1 \text{ kcal/mol}) \approx 0.1 \text{ ps}$$

Note that for an Arrhenius-type expression the rate constant depends on the preexponential factor, normally assumed to be ∼10^{13} s^{-1}:

$$k_{\mathrm{H}}{}^{-1}(\text{Arrhenius; 300 K; } \nu_{\mathrm{N-H}}) \approx 0.1 \text{ ps}$$

$$k_{\mathrm{H}}{}^{-1}(\text{Arrhenius; 300 K; } \nu_{\mathrm{N\cdots N}}) \approx 3 \text{ ps}$$

$$k_{\mathrm{H}}{}^{-1}(\text{Arrhenius; 300 K; } 10^{13} \text{ s}^{-1}) \approx 1 \text{ ps}$$

For D substitution, E_0^{D} = 900 cm^{-1}, a_0^{D} = 0.36 Å, $\nu_{\mathrm{N-D}}$ = 2000 cm^{-1}, and m_{D} = 2, we obtained:

$$k_{\mathrm{D}}{}^{-1}(E = 0) \approx 1 \text{ ns}$$

$$k_{\mathrm{D}}{}^{-1}(E \sim 1 \text{ kcal/mol}) \approx 80 \text{ ps}$$

$$k_{\mathrm{D}}{}^{-1}(\text{Arrhenius; 300 K; } \nu_{\mathrm{N-D}}) \approx 1.5 \text{ ps}$$

$$k_{\mathrm{D}}{}^{-1}(\text{Arrhenius; 300 K; } \nu_{\mathrm{N\cdots N}}) \approx 25 \text{ ps}$$

$$k_{\mathrm{D}}{}^{-1}(\text{Arrhenius; 300 K; } 10^{13} \text{ s}^{-1}) \approx 9 \text{ ps}$$

It should be realized that an Arrhenius-type behavior is valid when a temperature is defined, not microcanonically and especially when E = 0. If these details of the change in E_0 and a_0 upon deuteration are ignored, then the D effect is much different giving $k_{\mathrm{D}}{}^{-1}$ = 6 ps, i.e., an order of magnitude larger than the 0.6 ps value for H. The above trends reproduce the isolated pair rates as a function of E, but the isotope effect is predicted to be larger than the experimental one order of magnitude change. Of course, the above picture describes a one-dimensional tunneling dynamics and we must consider the N···N motion as well. Elsewhere,[17,39] we detailed such an effect by averaging k of eq A1 over the vibrational state of the N···N motion:[49] For E = 0, the zero-point vibrational motion results in the following values:

$$k^{-1}(\text{N−H, N···N}) \approx 0.5 \text{ ps}$$

$$k^{-1}(\text{N−D, N···N}) \approx 350 \text{ ps}$$

illustrating the influence on reducing the isotope effect; the reduced mass for the N···N motion (7-AI dimer) is taken to be 59. As shown in Figure 12, the N···N distance controls the barrier height and any calculation of the isotope effect must take into account the dynamics in the N−H and N···N nuclear space.

Note Added in Proof. In a recent paper from Castleman's group (D. E. Folmer et al., PNAS, to be published) the effect of water solvation in a molecular beam was studied for the reactive and nonreactive pairs. They showed that the dynamics in the reactive pair is a two-step process and that solvation by water facilitates the proton transfer in the nonreactive dimer.

References and Notes

(1) Watson, J. D.; Crick, F. H. C. *Nature* (*London*) **1953**, *171*, 964.
(2) (a) Jefrey, A.; Saenger, W. *Hydrogen Bonding in Biological Structures*; Springer-Verlag: Berlin, 1991. (b) Steenken, S. *Chem. Biol.* **1997**, *378*, 1293.
(3) Löwdin, P.-O. *Adv. Quantum Chem*. **1965**, *2*, 213.
(4) (a) Lehn J. M. *Supramolecular Chemistry: Concepts and Perspectives*; VCH Publishers: New York, 1995. (b) Zewail, A., Ed. *The Chemical Bond: Structure and Dynamics*; Academic: San Diego, CA, 1992. (c) Ball, P. *Designing the Molecular World*; Princeton University Press: Princeton, NJ, 1994.
(5) Taylor, C. A.; El-Bayoumi, M. A.; Kasha, M. *Proc. Natl. Acad. Sci. U.S.A.* **1969**, *63*, 253.
(6) Ingham, K. C.; Abu-Elgheit, M.; El-Bayoumi, M. A. *J. Am. Chem. Soc*. **1971**, *93*, 5023.
(7) Ingham, K. C.; El-Bayoumi, M. A. *J. Am. Chem. Soc*. **1974**, *96*, 1674.
(8) Bulska, G.; Grabowska, A.; Pakula, B.; Sepiol, J.; Waluk, J.; Wild, U. P. *J. Lumin.* **1984**, *29*, 65.
(9) Chen, Y.; Rich, R. L.; Gai, F.;. Petrich, J. W.*J. Phys. Chem*. **1993**, *97*, 1770.
(10) Tokomura, K.; Watanabe, Y.; Itoh, M. *Chem. Phys. Lett.* **1984**, *111*, 379.
(11) Tokomura, K.; Watanabe, Y.; Udagawa, M.; Itoh, M. *J. Am. Chem. Soc*. **1987**, *109*, 1346.
(12) Fuke, K.; Yoshiuchi, H. Kaya, K. *J. Phys. Chem.* **1984**, *88*, 5840.
(13) Fuke, K.; Kaya, K. *J. Phys. Chem.* **1989**, *93*, 614.
(14) Nakajima, M.; Hirano, R.; Hasumi, K.; Kaya, H.; Watanabe, C. C.; Carter, J. M.; Williamson, Miller, T. A. *J. Phys. Chem*. **1997**, *101*, 392.
(15) Hetherington, W. M. III; Micheels, R. H.; Eisenthal, K. B. *Chem. Phys. Lett.* **1979**, *66* 230.
(16) Share, P.; Pereira, M.; Sarisky, M.; Repinec, S.; Hochstrasser, R. M. *J. Lumin.* **1991**, *48/49*, 204.
(17) Douhal, A.; Kim, S. K.; Zewail, A. H. *Nature* **1995**, *378*, 260.
(18) Folmer, E.; Poth, L.; Wisniewski, E. S.; Castleman Jr., A. W. *Chem. Phys. Lett.* **1998**, *287*, 1.
(19) Lopez-Martens, R.; Long, P.; Solgadi, D.; Soep, B.; Syage, J.; Millie, Ph. *Chem. Phys. Lett.* **1997**, *273*, 219.
(20) Douhal, A.; Guallar, V.; Moreno, M.; Lluch, J. M. *Chem. Phys. Lett.* **1996**, *256*, 370.
(21) Guallar, V.; Moreno, M.; Lluch, J. M. *Chem. Phys. Lett.* **1998**, *228*, 1.
(22) Guallar, V.; Batista V.; Miller, W. H., *J. Chem. Phys*. **1999**, *110*, 9922.
(23) Takeuchi, S.; Tahara, T. *Chem. Phys. Lett.* **1997**, *227*, 340.
(24) Takeuchi, S. Tahara, T. *J. Phys. Chem*. **1998**, *102*, 7740.
(25) Chachisvilis, M.; Fiebig, T.; Douhal, A.; Zewail, A. H. *J. Phys. Chem. A* **1998**, *102*, 669.
(26) Robinson, M. M.; Robinson, B. L, *J. Am. Chem. Soc.* **1955**, *77*, 6554.
(27) Møller, K.; Zewail, A. H. *Chem. Phys. Lett*. **1998**, *298*, 1.
(28) (a) Diau, E. W. G.; Abou-Zied, O. K.; Scala, A. A.; Zewail, A. H. *J. Am. Chem. Soc.* **1998**, *120*, 3245. (b) De Feyter S.; Diau, E. W. G.; Scala, A. A.; Zewail, A. H. *Chem. Phys. Lett.* **1999**, *303*, 249. (c) Diau, E. W. G.; De Feyter S.; Zewail, A. H. *Chem. Phys. Lett.* **1999**, *304*, 134.
(29) Catalan, J.; Perez, P. *J. Theor. Biol.* **1979**, *81*, 213.
(30) Kim, S. K.; Bernstein, E. R. *J. Phys. Chem.* **1990**, *94*, 3531.
(31) Ilich, P. *J. Mol. Struct.* **1995**, *354*, 37.
(32) Shukla, M. K.; Mishra, P. C. *Chem. Phys.* **1998**, *230*, 187.

(33) Chou, P.-T.; Wei, C.-Y.; Chang, C.-P.; Meng-Shin, K. *J. Phys. Chem*. **1995**, *99*, 11994.

(34) Foresman, J. B.; Head-Gordon, M.; Pople, J. A.; Frisch, M. J., *J. Phys. Chem*. **1992**, *96*, 135.

(35) Frisch, M. J.; Trucks, G. W.; Schlegel, H. B.; Gill, P. M. W.; Johnson, B. G.; Robb, M. A.; Cheeseman, J. R.; Keith, T. A.; Petersson, J. A.; Montgomery, K.; Raghavachari, K.; Al-Laham, M. A.; Zakrewski, V. G.; Ortiz, J. V.; Foresman, J. B.; Cioslowski, J.; Stefanov, B. B.; Nanayakkara, A.; Challacombe, M.; Peng, C. Y.; Ayala, W.; Chen, W.; Wong, M. W.; Andres, J. L.; Replogle, E. S.; Gomperts, R.; Martin, R. L.; Fox, D. J.; Binkley, J. S.; Defrees, D. J.; Baker, J.; Stewart, J. P, Head-Gordon, M.; Gonzalez, C.; Pople, J. A. *Gaussian 94*; Gaussian Inc.: Pittsburgh, PA, 1995.

(36) Hynes, J. T.; Borgis, D, *J. Phys. Chem*. **1996**, *100*, 1118.

(37) Felker, P. M.; Zewail, A. H. *J. Phys. Chem.* **1985**, *89*, 5402.

(38) Lee, S.; Hynes J. T. *J. Chim. Phys. Biol*. **1996**, *93*, 1783.

(39) Kim, S. K.; Breen, J. J.; Willberg, D. M.; Peng, L. W.; Heikal A.; Syage, J. A.; Zewail, A. H. *J. Phys. Chem.* **1995**, *99*, 7421, and references therein.

(40) Douhal, A.; Lahmani, F.; Zewail, A. H. *Chem. Phys.* **1996**, *207*, 477.

(41) T. Bountis, ed. *Proton Transfer in Hydrogen-Bonded Systems*; Plenum: New York, 1992.

(42) Wan, P., Shukla D. *Chem. Rev.* **1993**, *93*, 571.

(43) Marks, D.; Prosposito, P.; Zhang, H.; Glasbeek, M. *Chem. Phys. Lett.* **1998**, *289*, 535.

(44) Saltiel, J.; D'Agostino, J.; Megarity, E. D.; Metts, L.; Neuberger, K. R.; Wrighton, M.; Zafiriou, O. C. *Org. Photochem*. **1973**, *3*, 1.

(45) Roos, B. O. *Acc. Chem. Res.* **1999**, *32*, 137.

(46) Babamov, V. K.; Marcus, R. A. *J. Chem. Phys.* **1981**, *74*, 1790.

(47) Cukier, R. I.; Zhu, J. *J. Chem. Phys.* **1999**, *110*, 9587, and references therein.

(48) Alben, J. O.; Beece, D.; Bowne, S. F.; Eisenstein, L.; Frauenfelder, H.; Good, D.; Marden, M. C.; Moh, P. P.; Reinisch, L. Reynolds, A. H.; Yue, K. T. *Phys. Rev. Lett*. **1980**, *44*, 1157.

(49) Hineman, M. F.; Brucker, G. A.; Kelley, D. F.; Bernstein, E. R. *J. Chem. Phys.* **1992**, *97*, 3341.